Acta Crystallographica Section D
Biological Crystallography
ISSN 1399-0047

Protein–RNA affinity of ribosomal protein L1 mutants does not correlate with the number of intermolecular interactions

Svetlana Tishchenko,[a] Olga Kostareva,[a,b] Azat Gabdulkhakov,[a] Alisa Mikhaylina,[a] Ekaterina Nikonova,[a] Natalia Nevskaya,[a] Alena Sarskikh,[a,b] Wolfgang Piendl,[b] Maria Garber[a] and Stanislav Nikonov[a]*

[a]Institute of Protein Research, Russian Academy of Sciences, Institutskaya 4, 142290 Pushchino, Moscow Region, Russian Federation, and [b]Biocenter, Division of Medical Biochemistry, Innsbruck Medical University, Innrain 80–82, 6020 Innsbruck, Austria

Correspondence e-mail: nikonov@vega.protres.ru

Received 22 August 2014
Accepted 29 November 2014

PDB references: TthL1, T217V mutant, 4reo; T217V mutant, DNA complex, 3u56; G219V mutant, 4qgb; G219V mutant, DNA complex, 4qg3; T217A mutant, DNA complex, 3umy; M218L mutant, DNA complex, 4qvi

Ribosomal protein L1, as part of the L1 stalk of the 50S ribosomal subunit, is implicated in directing tRNA movement through the ribosome during translocation. High-resolution crystal structures of four mutants (T217V, T217A, M218L and G219V) of the ribosomal protein L1 from *Thermus thermophilus* (TthL1) in complex with a specific 80 nt fragment of 23S rRNA and the structures of two of these mutants (T217V and G219V) in the RNA-unbound form are reported in this work. All mutations are located in the highly conserved triad Thr-Met-Gly, which is responsible for about 17% of all protein–RNA hydrogen bonds and 50% of solvent-inaccessible intermolecular hydrogen bonds. In the mutated proteins without bound RNA the RNA-binding regions show substantial conformational changes. On the other hand, in the complexes with RNA the structures of the RNA-binding surfaces in all studied mutants are very similar to the structure of the wild-type protein in complex with RNA. This shows that formation of the RNA complexes restores the distorted surfaces of the mutant proteins to a conformation characteristic of the wild-type protein complex. Domain I of the mutated TthL1 and helix 77 of 23S rRNA form a rigid body identical to that found in the complex of wild-type TthL1 with RNA, suggesting that the observed relative orientation is conserved and is probably important for ribosome function. Analysis of the complex structures and the kinetic data show that the number of intermolecular contacts and hydrogen bonds in the RNA–protein contact area does not correlate with the affinity of the protein for RNA and cannot be used as a measure of affinity.

1. Introduction

Ribosomal protein L1, as part of the L1 stalk of the 50S ribosomal subunit, is implicated in directing tRNA movement through the ribosome during translocation (Fei *et al.*, 2009; Trabuco *et al.*, 2010). The protein consists of two domains and binds helices 76, 77 and 78 of 23S rRNA with high affinity (Nevskaya *et al.*, 2005). Analysis of the crystal structures of the complexes formed by the protein or its isolated domain I with 23S rRNA and mRNA fragments (Nikulin *et al.*, 2003; Nevskaya *et al.*, 2006; Tishchenko *et al.*, 2006, 2008) shows that the loop between β-strands β9 and β10 (Fig. 1*a*) that contains the universally conserved triad Thr-Met-Gly plays an important role in RNA binding. This triad, which comprises only 11% of all interacting residues, is involved in 20% of the RNA–protein contacts within a region of up to 4.0 Å, and about 40% of these contacts are formed by threonine (Kostareva *et al.*, 2011). Such a tight contact area is suitable for studying the

effect of strain-relief modifications at the protein–RNA interface on the RNA-binding properties of L1. The available structures also show that the side-chain hydroxyl and main-chain carbonyl groups of the threonine residue as well as the main-chain carbonyl group of the glycine residue form hydrogen bonds to polar RNA atoms which are inaccessible to solvent. By replacement of the amino-acid residues within this region it should be possible to gain further insight into the mechanism of RNA–protein recognition and RNA binding by the protein. This would require the structures of mutant proteins both in complex with RNA and without RNA, with corresponding amino-acid mutations.

The structure of RNA-free bacterial L1 is characterized by a closed conformation (Nikonov *et al.*, 1996; Nikonova *et al.*, 2007; Tishchenko *et al.*, 2011), with the two domains in close proximity to each other but with an unusually small number of contacts between the domains. On the other hand, in the RNA-bound form the two domains are separated from each other and show an open conformation (Nevskaya *et al.*, 2006). The open and closed conformations of L1 from *Thermus thermophilus* (TthL1) and the conformational changes in the RNA-binding region upon RNA binding are shown in Supplementary Figs. S1 and S2, respectively. Archaeal L1 has an open conformation in both the unbound and RNA-bound forms (Nevskaya *et al.*, 2000, 2005).

We have previously determined the crystal structures of several RNA-free mutants of L1 from *T. thermophilus* and *Methanococcus jannaschii* (MjaL1) with substitutions of key RNA-binding residues (Nikonova *et al.*, 2007) and studied the affinity of some of them for a specific 23S rRNA fragment (Kostareva *et al.*, 2011). It was shown that in some cases the mutations induced significant alterations in the region of the protein structure responsible for RNA binding. Kinetic experiments showed that some of these mutants were still able to specifically recognize the 23S rRNA fragment, although the complexes showed very low stability (Kostareva *et al.*, 2011).

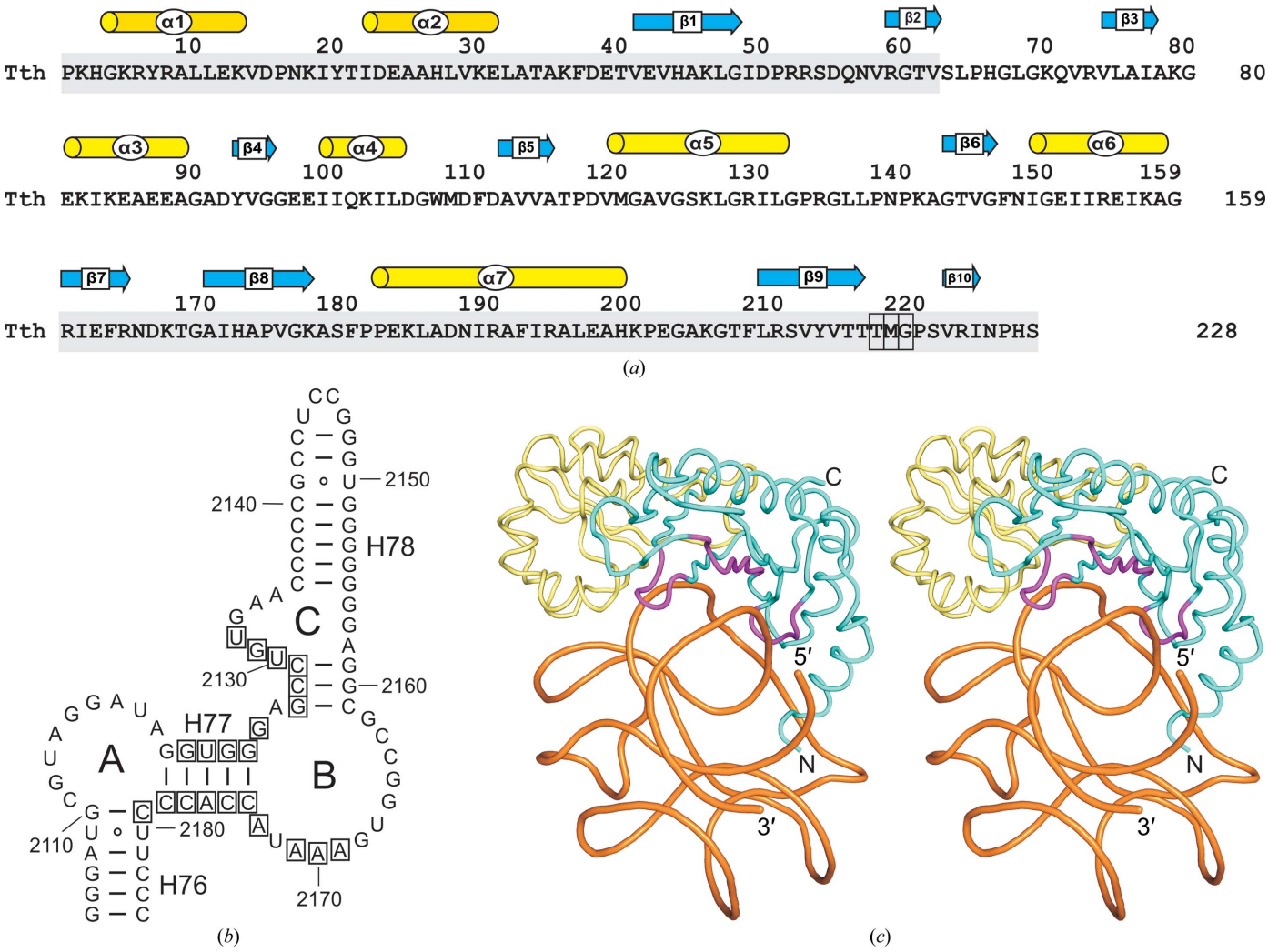

Figure 1
Constituents of the TthL1–rRNA complex. (*a*) Sequence of L1 from *T. thermophilus*. α-Helices are shown as yellow cylinders and β-strands as blue arrows. Mutated residues are boxed. Domain I is shown with a grey background. (*b*) Secondary structure of the 80 nt 23S rRNA fragment from *T. thermophilus*. Sequence positions and helices are numbered according to *E. coli* 23S rRNA. Nucleotides that interact specifically with TthL1 are boxed. (*c*) Stereoview of the TthL1–rRNA complex. The protein is shown in yellow (domain I) and cyan (domain II) and rRNA is shown in gold. Loops β7–β8, β9–β10 and strand β1 of domain I forming the 'tongs' are shown in magenta.

In these experiments we used a specific 23S rRNA fragment containing helix 77, shortened versions of helices 76 and 78, and the interconnecting loops A and B (Nikulin *et al.*, 2003). Our attempts to obtain crystals of L1 mutants in complex with this incomplete RNA fragment of the L1 stalk were unsuccessful.

Recently, we succeeded in determining the high-resolution crystal structure of the reconstructed full-length ribosomal L1 stalk (Tishchenko *et al.*, 2012), consisting of ribosomal protein TthL1 and a specific 80-nucleotide 23S rRNA fragment including the entire helix 78 (Fig. 1*b*). The presence of this helix in the complex provided additional RNA–protein contacts and intermolecular RNA–RNA contacts within the crystal that allowed us to obtain a high-resolution model. Subsequent use of the same RNA fragment resulted in the crystallization of several L1 mutants in the RNA-bound form.

Here, we report the high-resolution crystal structures of four mutants of TthL1 (T217A, T217V, M218L and G219V) in complex with the 80 nt fragment of 23S rRNA. Two of the mutants (T217V and G219V) were also crystallized in the free form without bound RNA. Compared with the wild-type protein, the structures of the RNA-free T217V and G219V mutants show conformational differences within the RNA-binding regions. On the other hand, in the RNA-bound form these regions adapt to the RNA surface and form RNA–protein interfaces similar to those observed in the wild-type TthL1–rRNA complex. Domain I of the protein and helix 77 of the 23S rRNA form a rigid-body structure identical to the wild-type complex structure and other studied complexes. The data suggest that the relative orientation of domain I and helix 77 is highly conserved and is probably important for ribosome function. Comparison of structural and kinetic data shows that the number of intermolecular contacts and hydrogen bonds in the protein–RNA contact areas in the studied L1 mutants does not correlate with the affinity of the protein for RNA. Kinetic data also suggest that some changes of structures introduced by the mutations are overcome through the formation of an intermediate complex.

2. Materials and methods

2.1. Plasmid constructs

The construct of the plasmid used as a template for the transcription of the 80 nt *T. thermophilus* rRNA fragment (Tth rRNA) has been described previously (Tishchenko *et al.*, 2012). The plasmids used for the production of wild-type TthL1 and its mutants T217A TthL1 and M218L TthL1 have been described in Nikonova *et al.* (2007). The QuikChange method was used for site-directed mutagenesis (Liu & Naismith, 2008) to clone TthL1 genes with Thr217 and Gly219 replaced by Val. The plasmid pTthL1.4 (Tishchenko *et al.*, 2007), carrying the TthL1 gene, was used as a PCR template. The genes of TthL1 mutants (T217V and G219V) were cloned into the expression vector pET-11a-PL. The nucleotide sequences of the cloned genes were verified by sequencing.

2.2. Protein and RNA preparation

TthL1 mutants (T217V, T217A, M218L and G219V) were overproduced in *Escherichia coli* BL21(DE3) cells. The proteins were purified as described previously (Nikonov *et al.*, 1996). Purified proteins for crystallization with RNA were dialyzed into a buffer consisting of 350 m*M* NaCl, 50 m*M* Tris–HCl (pH 7.5 at 298 K), 5 m*M* $MgCl_2$ and concentrated to 5–6 mg ml^{-1} using Vivaspin concentrators. The 80 nt Tth rRNA fragment was obtained as described in Tishchenko *et al.* (2012). To form protein–RNA complexes, the RNA fragment and the proteins were mixed in equimolar concentrations and incubated for 30 min at room temperature.

2.3. Crystallization

All crystallization experiments were performed at room temperature in Linbro plates using the hanging-drop vapour-diffusion method on siliconized glass cover slides.

2.3.1. Crystallization of the TthL1 T217V mutant. The protein was dialyzed into a buffer consisting of 40 m*M* glycine–NaOH pH 10.0, 4%(*v*/*v*) 2-methyl-2,4-pentanediol (MPD), 26% saturated ammonium sulfate and concentrated to 10 mg ml^{-1} using Vivaspin concentrators. 8 µl drops of the protein solution were equilibrated against 55% saturated ammonium sulfate with 6% MPD. Crystals appeared after 2 d and grew to maximum dimensions of 0.4 × 0.2 × 0.2 mm within one week. Prior to cooling in liquid nitrogen, the crystals were transferred into a solution composed of 60% saturated ammonium sulfate and 30% sucrose.

2.3.2. Crystallization of the TthL1 G219V mutant. The protein was dialyzed into a buffer consisting of 30 m*M* Tris–HCl (pH 7.5 at 298 K), 200 m*M* NaCl and concentrated to 20 mg ml^{-1} using Vivaspin concentrators. Drops were made by mixing 3 µl G219V TthL1 with 1 µl of a solution consisting of 2 *M* ammonium sulfate, 0.1 *M* sodium acetate pH 4.6 (condition No. 1.35 of JCSG-plus from Molecular Dimensions) and 0.5 µl 0.65% polyacrylic acid 5100 sodium salt. Drops were equilibrated against 1.8 *M* ammonium sulfate, 0.1 *M* sodium acetate pH 4.6. Crystals appeared after 5–6 d and grew to maximum dimensions of 0.8 × 0.2 × 0.2 mm within two weeks. Prior to cooling in liquid nitrogen, the crystals were transferred into a solution composed of 60% saturated ammonium sulfate and 30% sucrose.

2.3.3. Crystallization of RNA–protein complexes. The RNA fragment was heated at 333 K for 10 min and incubated for 10 min at 277 K. To form L1–RNA complexes, preparations of the RNA fragment and the protein were mixed in equimolar amounts and incubated for 30 min at room temperature.

2.3.4. Crystallization of the TthL1 T217V mutant in complex with rRNA. Drops were made by mixing 2 µl of the complex solution with 2 µl well solution (2.4 *M* sodium malonate pH 7.0). Crystals appeared in 3–5 d and grew to maximum dimensions of 0.05 × 0.15 × 0.3 mm within one week. Prior to cooling in liquid nitrogen, the crystals were transferred into the well solution.

Table 1
Data-collection and refinement statistics.

Values in parentheses are for the highest resolution shell.

	T217V TthL1	T217V TthL1–RNA	T217A TthL1–RNA	G219V TthL1	G219V TthL1–RNA	M218L TthL1–RNA
Data collection						
Radiation source	BL14.1, BESSY	Proteum X8	Proteum X8	Proteum X8	Proteum X8	Proteum X8
Wavelength (Å)	0.91841	1.5418	1.5418	1.5418	1.5418	1.5418
Temperature (K)	100	110	110	110	110	110
Space group	$P2_12_12$	$P2_12_12_1$	$P2_12_12_1$	$P2_12_12_1$	$P2_12_12_1$	$P2_12_12_1$
Unit-cell parameters (Å)						
a	75.99	73.69	67.11	66.53	72.77	73.14
b	60.45	75.41	68.82	74.75	76.48	75.84
c	43.75	85.88	88.83	87.06	86.25	86.50
Resolution (Å)	20.70–1.35 (1.42–1.35)	28.3–2.10 (2.20–2.10)	27.20–1.90 (2.00–1.90)	40.00–2.60 (2.69–2.60)	22.9–2.00 (2.10–2.00)	27.20–1.90 (2.00–1.90)
Measured reflections	177960 (24668)	129658 (13221)	116031 (16005)	30378 (737)	175339 (13121)	178598 (15427)
Unique reflections	44873 (6241)	28142 (3292)	32762 (4556)	12916 (1152)	33152 (4418)	38405 (5338)
Completeness (%)	99.6 (100.0)	98.5 (90.0)	98.9 (98.2)	93.2 (89.5)	99.6 (99.3)	99.3 (98.0)
Averaged multiplicity	3.96 (3.95)	4.60 (4.01)	3.54 (3.51)	2.23 (1.64)	5.27 (2.97)	4.62 (2.89)
$R_{\rm merge}$ (%)	2.5 (38.8)	9.9 (40.8)	10.4 (48.6)	11.8 (25.8)	6.7 (35.2)	6.4 (50.2)
Average $I/\sigma(I)$	25.16 (3.53)	12.57 (3.38)	10.99 (2.73)	7.50 (2.48)	13.81 (2.67)	13.40 (2.21)
Mosaicity (°)	0.23	0.24	0.30	0.64	0.51	0.47
Refinement						
Resolution (Å)	19.9–1.35 (1.38–1.35)	28.3–2.10 (2.17–2.10)	27.2–1.90 (1.96–1.90)	36.5–2.60 (2.80–2.60)	22.9–2.00 (2.06–2.00)	23.4–1.90 (1.95–1.90)
No. of reflections	44840 (4423)	28129 (2591)	32743 (2680)	12904 (2318)	31564 (2637)	37533 (2546)
R factor (%)	16.7 (23.6)	19.1 (27.6)	19.6 (27.5)	22.6 (27.6)	19.9 (28.7)	19.4 (27.9)
Free *R* factor (%)	20.9 (28.4)	23.8 (29.8)	24.6 (32.4)	25.1 (29.5)	22.6 (32.6)	21.7 (29.3)
Overall *B* factor (Å^2)	21.8	27.7	22.8	33.2	19.8	25.5
Coordinate error	0.14	0.28	0.51	0.21	0.24	0.21
Residues in the model	8–228	1–228	1–228	13–228	1–228	1–228
R.m.s. deviations						
Bond lengths (Å)	0.006	0.006	0.009	0.011	0.009	0.006
Bond angles (°)	1.116	0.935	1.139	1.577	1.247	1.027
Ramachandran plot						
Most favoured (%)	95.6	92.6	92.1	92.5	90.0	96.5
Additionally allowed (%)	4.4	7.4	7.9	7.5	10.0	3.5
PDB code	4reo	3u56	3umy	4qgb	4qg3	4qvi

2.3.5. Crystallization of the TthL1 T217A mutant in complex with rRNA. Hanging drops were made by mixing 2 µl of the RNA–protein complex solution with 2 µl well solution consisting of 2 *M* ammonium sulfate, 0.1 *M* bis-tris pH 6.5 (condition No. 4 of Index from Hampton Research). Crystals appeared after 3–4 d and grew to maximum dimensions of 0.1 × 0.2 × 0.4 mm within 1–2 weeks. Prior to cooling in liquid nitrogen, the crystals were transferred into 2.4 *M* sodium malonate pH 7.0.

2.3.6. Crystallization of the TthL1 M218L mutant in complex with rRNA. Drops were made by mixing 2 µl of the complex solution with 2 µl well solution consisting of 2.5 *M* ammonium sulfate, 0.05 *M* MES pH 5.6, 0.01 *M* magnesium acetate (condition No. 2 of Natrix from Hampton Research) and 0.5 µl 4% polyacrylic acid 5100 sodium salt. Crystals appeared in 3–4 d and grew to maximum dimensions of 0.06 × 0.15 × 0.40 mm within two weeks. Prior to cooling in liquid nitrogen, the crystals were transferred into a solution composed of 60% saturated ammonium sulfate and 30% sucrose.

2.3.7. Crystallization of the TthL1 G219V mutant in complex with rRNA. Drops were made by mixing 2 µl of the complex solution with 2 µl well solution consisting of 1.8 *M* ammonium sulfate, 0.05 *M* Tris–HCl (pH 8.5 at 298 K), 0.025 *M* magnesium sulfate (condition No. 45 of Natrix from Hampton Research). Crystals appeared in 2–3 d and grew to maximum dimensions of 0.05 × 0.10 × 0.30 mm within one week. Prior to cooling in liquid nitrogen, the crystals were transferred into 2.4 *M* ammonium sulfate, 0.05 *M* Tris–HCl (pH 8.5 at 298 K).

2.4. Data collection and structure determination

Diffraction data were collected from a single crystal in each experiment using an in-house Proteum X8 generator (Bruker) equipped with a MAR345 image-plate detector (MAR Research, Germany) or a Bruker PLATINUM[135] CCD detector (http://www.bruker.com). In addition, data were collected on beamline BL14.1, BESY, Berlin, Germany using a MAR225 CCD detector. Data were processed and merged using the *XDS* (Kabsch, 2010) or *PROTEUM*2 (http://www.bruker.com) packages.

The structures were solved by molecular replacement with *Phaser* (McCoy *et al.*, 2005) using TthL1 S179C (PDB entry 1ad2; Unge *et al.*, 1997) as a search model for isolated proteins and the model of the wild-type protein in complex with RNA (PDB entry 3u4m; Tishchenko *et al.*, 2012) as a search model for the RNA complexes. The initial models were subjected to crystallographic refinement, initially with *REFMAC*5 (Murshudov *et al.*, 2011) and subsequently with *PHENIX*

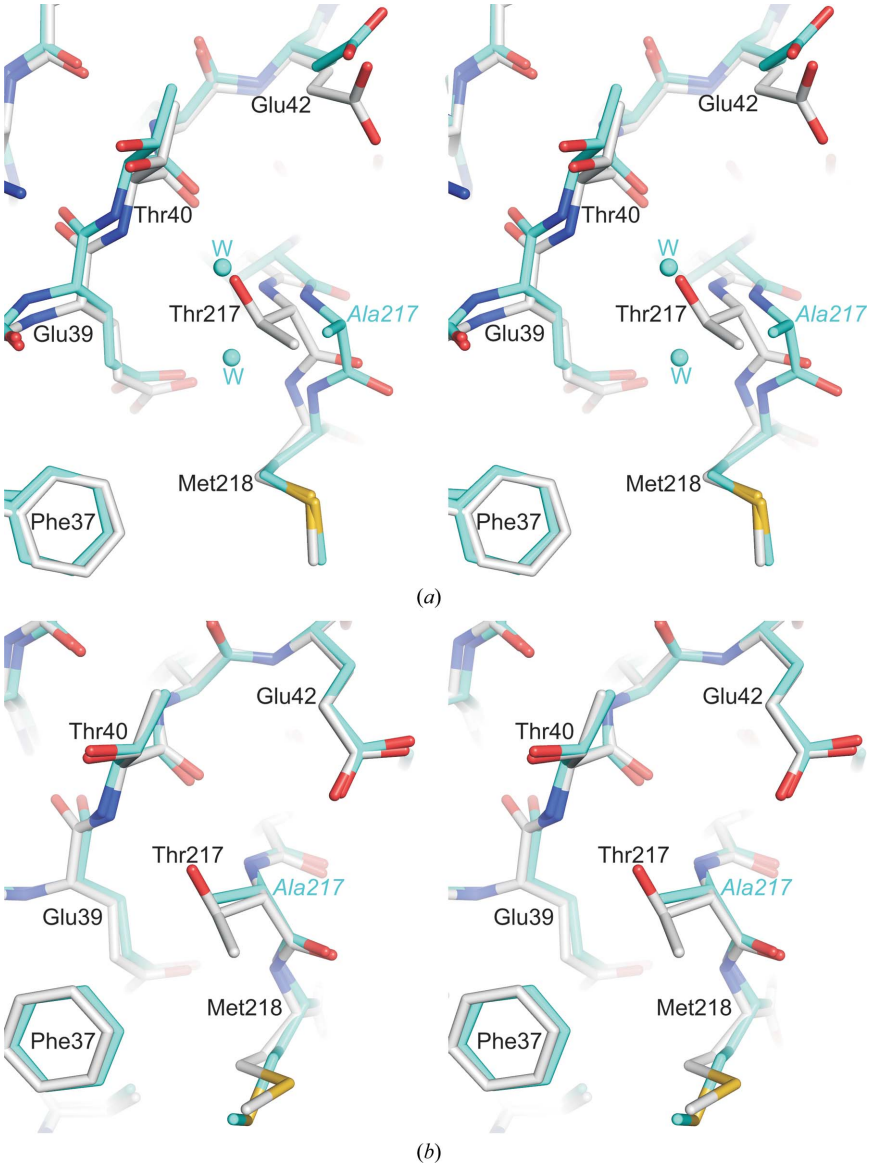

Figure 2
Superposition of the protein–RNA contact regions in wild-type TthL1 (C atoms in grey) and T217A mutant TthL1 (C atoms in blue) in RNA-free (*a*) and RNA-bound (*b*) forms. Replacement of Thr217 by Ala permits two associated water molecules between loops $\alpha2$–$\beta1$ and $\beta9$–$\beta10$ in the RNA-free mutant molecule. In the RNA-bound T217A TthL1, the RNA-binding region of the protein is in the same conformation as that observed in the RNA-bound wild-type TthL1. A small cavity can be observed in the flat surface formed by Phe37, Thr40, Glu42 and Met218.

(Afonine *et al.*, 2012). Manual rebuilding of the models was carried out in *Coot* (Emsley *et al.*, 2010). As in the wild-type structure, the N-terminal residues were very flexible in the RNA-free mutants and could not be traced in the electron-density map (Table 1). The quality of all of the models was checked using *PROCHECK* (Laskowski *et al.*, 1993) and *WHATCHECK* (Hooft *et al.*, 1996); no residues were detected in disallowed regions. Data-collection and refinement statistics are summarized in Table 1. The coordinates and structure factors have been deposited in the Protein Data Bank. Figures were prepared using *PyMOL* (http://www.pymol.org).

2.5. SPR experiments

SPR experiments were performed at the Human Proteome Shared Facility Center of the Institute of Biomedical Chemistry, Moscow, Russia and the Scientific Instrumentation Facility of Pushchino Research Center 'Structural and Functional Studies of Biological Systems', Pushchino, Russia. Real-time monitoring of the interactions of wild-type and mutant L1 proteins with the 23S rRNA fragment containing the specific L1 binding site was performed by SPR experiments (Katsamba *et al.*, 2002) using the ProteOn XPR36 Protein Interaction Array System (Bio-Rad, USA). Binding experiments were performed as reported previously (Tishchenko *et al.*, 2012). Kinetic analysis was performed by globally fitting curves describing a simple 1:1 bimolecular model to the set of five sensorgrams.

3. Results

3.1. Comparison of T217A TthL1 crystal structures in the free form and in complex with RNA

The previously determined crystal structure of the isolated mutant T217A TthL1 had a closed conformation in which two associated water molecules replaced the $O^{\gamma1}$ and $C^{\gamma2}$ atoms of Thr217 (Kostareva *et al.*, 2011). Each of these molecules forms a 'classical' network of four hydrogen bonds, which presumably contribute to the stability of the distorted conformation of the RNA-binding region. Penetration of water molecules into the protein may trigger displacement of the C^{β} atom of Ala217 by up to 2.0 Å, which results in the formation of a bulge on the protein–RNA interface (Fig. 2*a*). In the closed conformation of the protein, domain II shields the region of the mutation, preventing water molecules from accessing it. However, bacterial and archaeal L1 bind RNA in the open conformation in which both domains are separated from each other, making the region of the mutation accessible to solvent and RNA (Nikulin *et al.*, 2003; Nevskaya *et al.*, 2006; Tishchenko *et al.*, 2012). In this conformation the water molecules in the vicinity of Ala217 are no longer trapped within the protein structure and may easily be displaced. The crystal structure of TthL1 T217A in complex with the 80 nt 23S rRNA fragment shows no associated water molecules in the vicinity of the mutated residue and no distortion of local protein conformation at the RNA-binding surface. Instead, the amino-acid replacement results in the

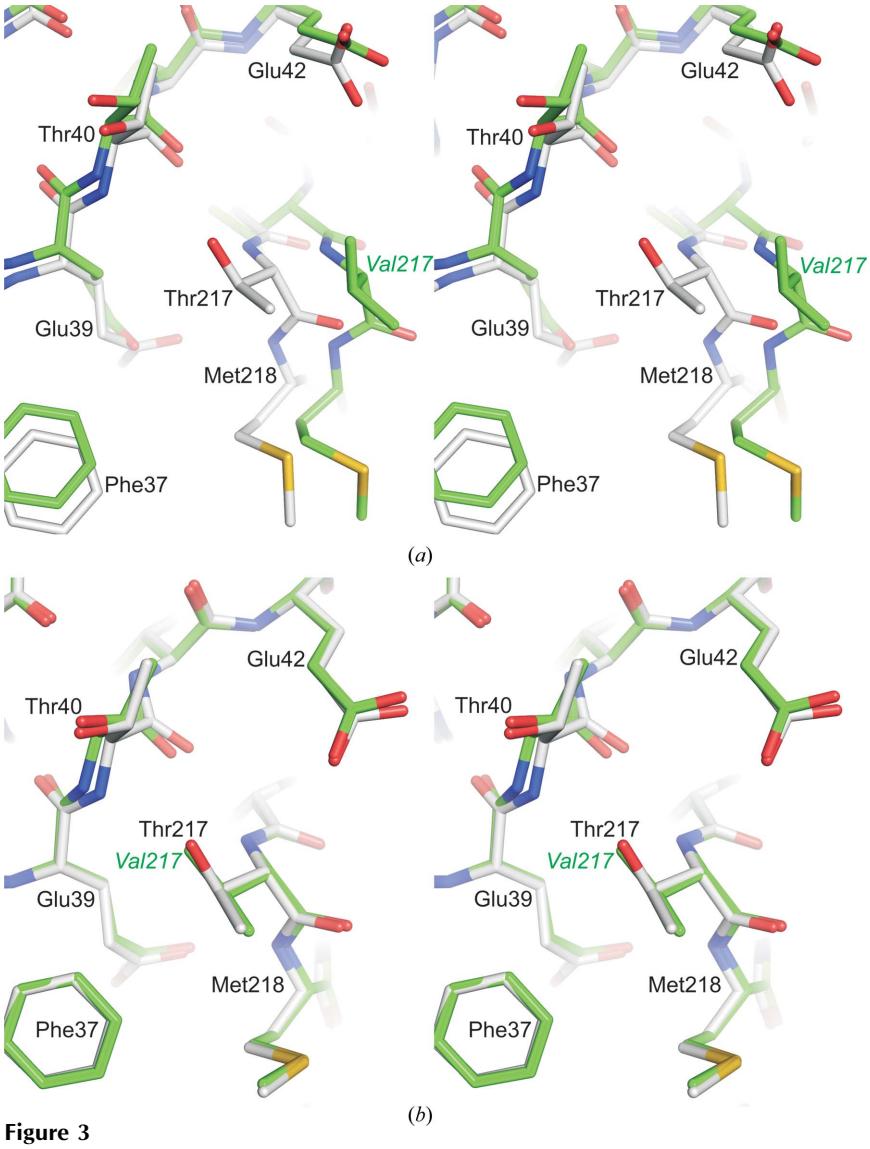

Figure 3
Superposition of the protein–RNA contact regions in the wild-type TthL1 (C atoms in grey) and T217V mutant TthL1 (C atoms in green) structures. (*a*) In the RNA-free form, the stereoview clearly shows that the T217V mutation shifts loop $\beta9$–$\beta10$ from its position in the wild-type protein. (*b*) In the complex, only the C^{α} and N atoms of Thr40 and the N atom of Val41 (loop $\alpha2$–$\beta1$) are shifted from their positions in the wild-type protein.

appearance of a small cavity in the flat surface formed by Phe37, Thr40, Glu42 and Met218 (Fig. 2*b*).

The structure of domain I (residues 1–67 and 160–228) in the RNA complex of the TthL1 T217A mutant is similar to the structure of domain I in the wild-type protein–RNA complex, showing a root-mean-square deviation (r.m.s.d.) of about 0.49 Å for all C^{α} atoms. Superposition of domains II (residues 68–159) yields an r.m.s.d. of 1.20 Å. The most significant conformational changes are observed in the $\beta4$–$\alpha4$–$\beta5$ region. Moreover, domain II of TthL1 T217A is shifted and rotated in relation to its position in the wild-type protein. As a result, the highly conserved Arg134 forms a hydrogen bond to RNA base G2123 instead of A2170, while Arg129 forms a cation–π interaction with the A2169 base.

The structures of the rRNA fragment in the mutant and wild-type complexes are also flexible (with an r.m.s.d. of 1.04 Å for the entire rRNA fragment). The most altered regions are helix 76, loop A, loop C and loop B. The position of helix 78 is slightly shifted relative to its position in the wild-type protein–RNA complex. Domain I of the protein and helix 77 of 23S rRNA retain their relative position: their superposition on the corresponding elements of the wild-type complex produces an r.m.s.d. of 0.48 Å.

3.2. Comparison of the T217V TthL1 crystal structures in the free form and in complex with RNA

The crystal structure of the isolated domain I of the TthL1 Thr217V mutant has been determined previously (Kostareva *et al.*, 2011). Here, the crystal structure of the entire TthL1 Thr217V mutant is presented and is compared with the structures of the isolated domain I of the entire wild-type TthL1. In the wild-type protein Thr217 forms a short hydrogen bond (2.4 Å) to the main-chain O atom of Pro133, which belongs to domain II. Replacement of the hydroxyl group of Thr217 by the methyl group of valine leads to a shift in the position of the loop between strands $\beta9$ and $\beta10$ (containing Thr217) away from domain II, which disrupts the hydrogen bond formed by the $O^{\gamma1}$ atom of Thr217 to the main-chain amide of Thr40. As a result, loop $\beta9$–$\beta10$ changes its position relative to the N-terminus of strand $\beta10$ and forms a bulge on the protein surface (Fig. 3*a*). Glu39 becomes accessible to solvent and loop $\alpha2$–$\beta1$, containing the universally conserved Phe37 that is important for RNA binding (Nevskaya *et al.*, 2006), acquires additional flexibility. It should be noted that domain II has an influence on the mutation-triggered conformational changes in the RNA-binding region of domain I; mutations in full-length L1 and in isolated domain I produce structures which can be superimposed with an r.m.s.d. of 1.35 Å. Most of the changes affected the position of loop $\beta9$–$\beta10$ and the conformation of loop $\alpha2$–$\beta1$.

We have also determined the crystal structure of this mutant of the protein in complex with the 80 nt 23S rRNA fragment which was previously used in the reconstruction of the full-length ribosomal L1 stalk. Similarly to the RNA-bound wild-type TthL1, the RNA-bound T217V mutant demonstrates an open conformation with a slightly different arrangement of the two domains. Unexpectedly, the distortion of the structure of the RNA-binding surface of the RNA-free protein could not be observed in the RNA-bound form. The bulge on the surface was absent and loops $\alpha2$–$\beta1$ and $\beta9$–$\beta10$ occupied a

position similar to that found in the RNA-bound wild-type protein. Comparison of the mutant and wild-type complexes yields an r.m.s.d. of 0.32 Å for all C^{α} atoms of domain I, while the structure of the whole rRNA fragment yields an r.m.s.d. of 1.27 Å. Superposition of the structures of the entire domain I of the T217V mutant and helix 77 of the bound rRNA fragment on the structure of the wild-type complex produces an r.m.s.d. of 0.35 Å. This confirms that, similar to the previous case, domain I of T217V TthL1 and helix 77 behave like a single rigid body identical to that formed in the wild-type protein complex, with similar conformations of the protein–RNA interfaces. To compensate for the increase in size caused by the replacement of the hydroxyl group of Thr217 by the methyl group of valine, a small deformation of the contact surface occurs on complex formation. Thus, retention of complementarity of the interacting surfaces of the protein and RNA results in shifts in the main-chain N and C^{α} atoms of Thr40 and the N atom of Val41 (Fig. 3*b*).

The entire domains II of the T217V mutant and the wild-type protein can be superimposed with an r.m.s.d. of 1.02 Å for all C^{α} atoms. Similarly to the T217A mutant, the $\beta4$–$\alpha4$–$\beta5$ region of the T217V mutant is also affected by the most significant conformational changes. The relative position of domains I and II is similar to that found in the wild-type complex.

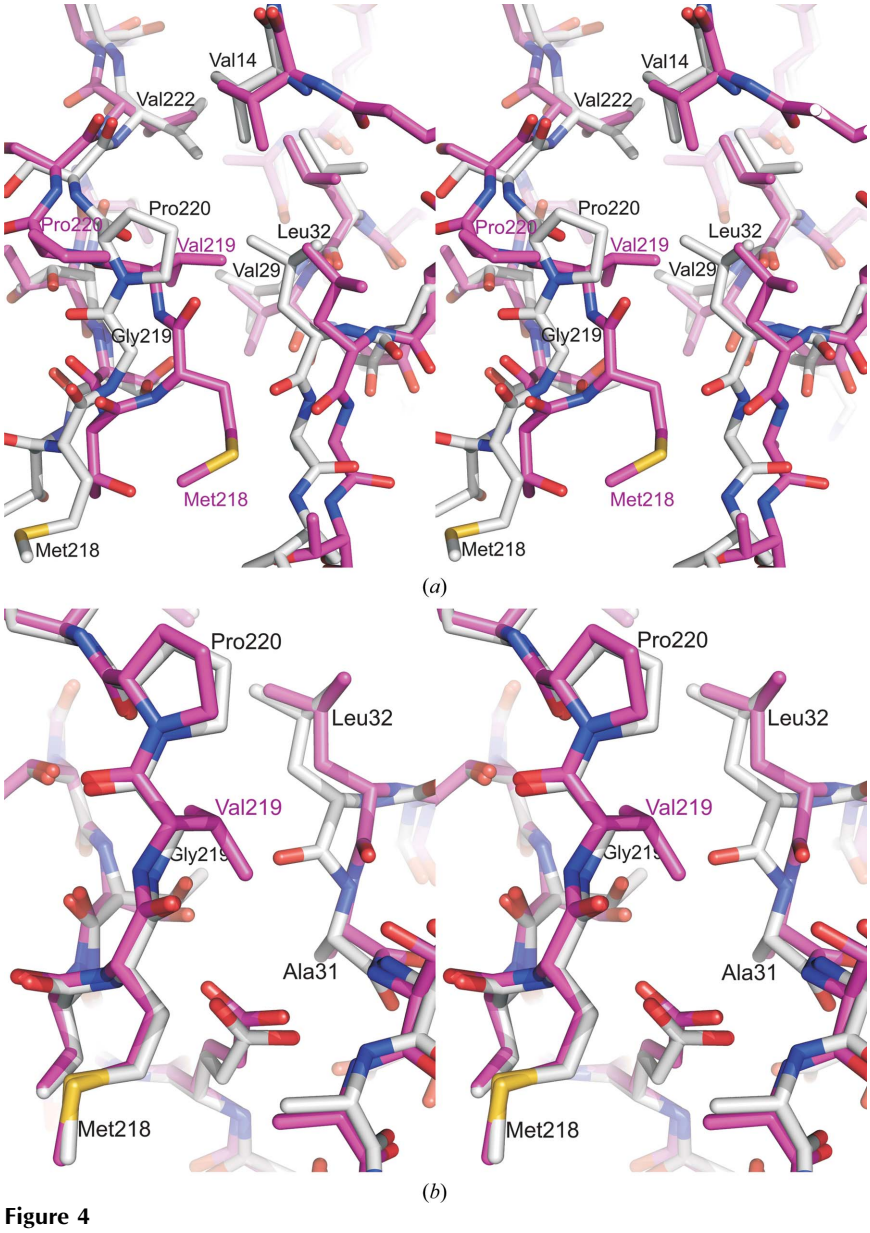

Figure 4
Superposition of the protein–RNA contact regions in the wild-type TthL1 (C atoms in grey) and G219V mutant TthL1 (C atoms in magenta) structures. (*a*) The stereoview clearly shows that in the RNA-free form the G219V mutation shifts loop $\beta9$–$\beta10$ from the corresponding position in the wild-type protein and changes its conformation. The S atom of Met218 as well as Pro220 are considerably displaced from their positions in the wild-type protein. The side chain of Val219 is inserted into the hydrophobic core formed by Val14, Val29, Leu32 and Val222. (*b*) In the G219V TthL1–rRNA complex, the side chain of Val219 occupies a position opposite to the Leu32-Ala33 main chain and changes its conformation.

3.3. Comparison of G219V TthL1 crystal structures in the free form and in complex with RNA

The structure of the G219V mutant was solved in a free form and in complex with RNA. In the free form of the structure, the introduction of Val219 into the hydrophobic core formed by Val14, Val29, Leu32 and Val222 causes significant changes not only in the position of loop $\beta9$–$\beta10$ but also in its conformation (Fig. 4*a*). The S atom of the side chain of Met218 is displaced by approximately 7 Å relative to its position in the wild-type protein, while Pro220 is displaced by 3 Å on average and forms a 3 Å bulge on the protein surface affecting the formation of intermolecular protein–RNA hydrogen bonds.

It is logical to suggest that this protein could lose its ability to form specific protein–RNA interactions. Nevertheless, a complex with the 80 nt fragment of 23S rRNA was obtained and its structure was determined. It is surprising that the structure of the protein–RNA interface in this complex is identical to that of the wild-type protein complex and all intermolecular hydrogen bonds are preserved. Some changes are found in the regions of the protein close to the protein–RNA interface: the side chain of the newly introduced Val219 is positioned opposite to the Leu32-Ala33 main-chain region and affects its conformation (Fig. 4*b*). In addition, it displaces the side chain of Thr216 and shifts the C-terminal part of helix $\alpha1$. The displacement of the $O^{\gamma1}$ atom of Thr216 by about 1.1 Å results in rearrangement of the intramolecular hydrogen bonds between loops $\alpha2$–$\beta1$ and $\beta9$–$\beta10$ (Supplementary Table S1).

The entire domain I, the rRNA fragment and part of the structure containing domain I and helix 77 of 23S rRNA in the G219V mutant complex can be superimposed on the corresponding regions of the wild-type protein complex with r.m.s.d.s of 0.40, 0.75 and 0.45 Å, respectively. This shows that domain I and helix 77 of the rRNA fragment in the complex formed by the TthL1 G219V mutant also make up a structure closely similar to that of the complex formed by wild-type TthL1. Domain II in this mutant occupies a position close to that of the wild-type protein complex. The highly conserved Arg134 occupies a similar position in both complexes. The superposition of domains II yields an r.m.s.d. of 1.19 Å and shows that the region α4–α5, which contains strand β4, is the most altered part of the domain.

3.4. Comparison of M218L TthL1 crystal structures in the free form and in complex with RNA

The structure of the TthL1 M218L mutant in the free form was solved some years ago at 2.0 Å resolution (Nikonova *et al.*, 2007). The crystals of this mutant show a very tight packing: their unit-cell volume is smaller by 10% compared with crystals of wild-type TthL1. This results in a closer distance between loops β7–β8 and β9–β10, both of which envelope helix 77 of rRNA in the complexes. In the region of the mutation, the side chain of Phe37 and the $C^{\delta1}$ and $C^{\delta2}$ atoms of Leu218, which are positioned in the same plane as the aromatic ring of Phe37, form an extensive hydrophobic patch. Compared with the wild-type protein, this patch changes the appearance and other features of the RNA-binding region (Fig. 5*a*). Moreover, hydrogen bonds formed by the $O^{\varepsilon1}$ atom of Glu39 to the main-chain amide of Met218 and the $O^{\gamma1}$ atom of Thr217 were broken (the distances between interacting atoms increased from 2.91 to 3.69 Å and from 3.00 to 5.10 Å, respectively). This may have caused a nonconcerted motion of loops α2–β1 and β9–β10.

We have also solved the crystal structure of the complex formed by the TthL1 M218L mutant and the 80 nt fragment of 23S rRNA. As expected, this structure is very similar to that formed by the wild-type protein and all examined mutants (Supplementary Table S2). The side chain of Leu218 essentially coincides with the side chain of Met218 in the wild-type TthL1–rRNA complex. The $C^{\delta2}$ atom of Leu218 occupies the position of the S^{δ} atom of the methionine and is able to form a C—H···O hydrogen bond to C2174 (Fig. 5*b*). The average *B* factors for the region highlighted in Figs. 2–5 are shown in Supplementary Table S3. The relative position of the domains and the conformation of domain II are very similar to those observed in the protein–RNA complexes formed by the T217V and G219V mutants.

3.5. Kinetic analysis of the interactions between TthL1 mutants and the 80 nt 23S rRNA fragment

The results of the present study show that the structures of the complexes of TthL1 mutants with RNA are very similar to

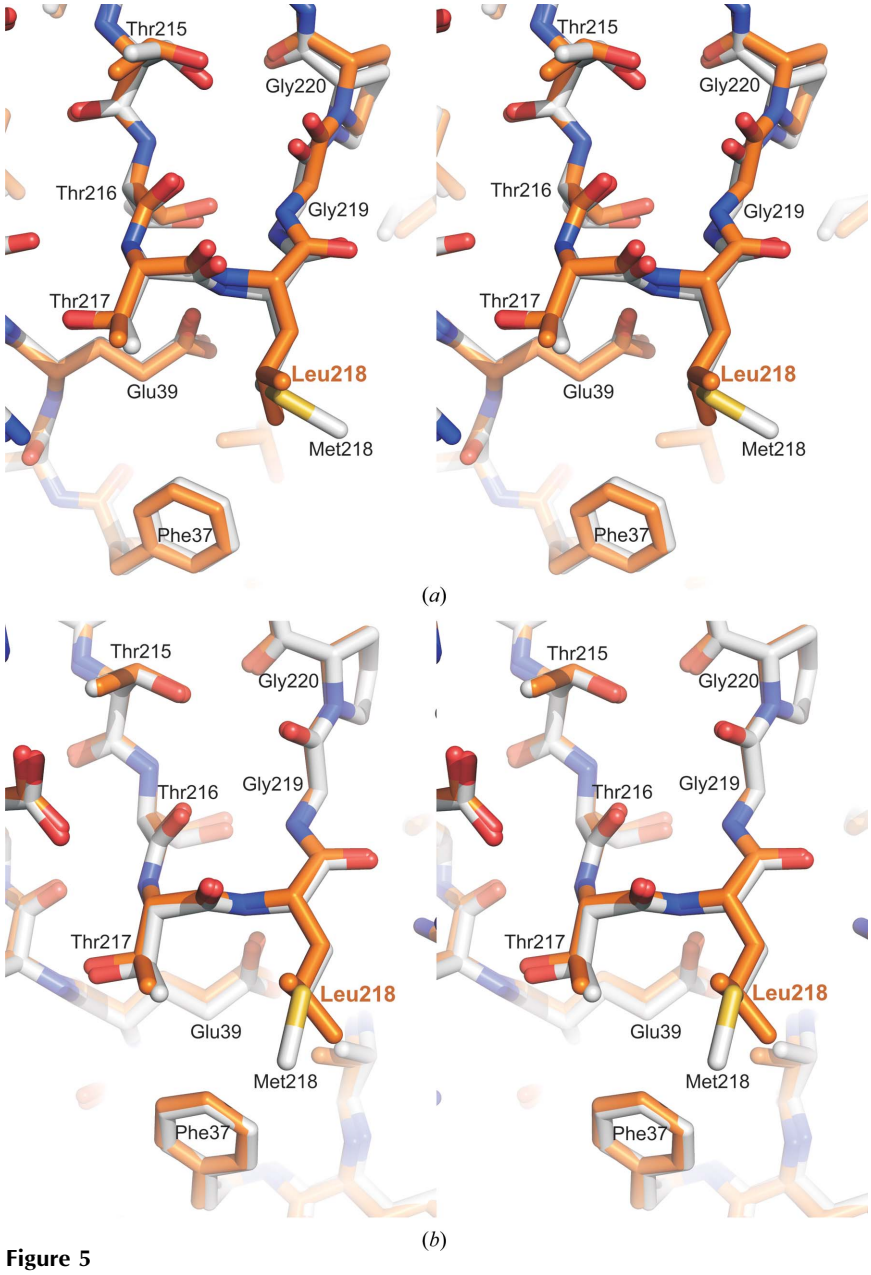

Figure 5
Superposition of protein–RNA contact regions in the wild-type TthL1 (C atoms in grey) and M218L mutant TthL1 (C atoms in orange) structures. (*a*) In the RNA-free form, the stereoview clearly shows that the side chains of Leu218 and Phe37 form a flat hydrophobic patch on the protein surface. (*b*) In the M218L TthL1–rRNA complex the side chain of Leu218 virtually matches the side chain of Met218 in the wild-type TthL1–rRNA complex

Table 2
Statistics of L1–RNA contact regions for protein–RNA distances in the interval 2.6–4.0 Å.

L1–RNA complex	Total No. of contacts	Average L1–RNA distance (Å)	No. of hydrogen bonds	No. of solvent-inaccessible hydrogen bonds	K_d (K_m) (M)
TthL1–RNA	244	3.586	20	6	2.14×10^{-12}
T217A TthL1–RNA	267	3.614	18	5	1.44×10^{-10}
T217V TthL1–RNA	262	3.585	19	5	9.79×10^{-10}
G219V TthL1–RNA	232	3.601	18	6	1.87×10^{-8}
M218L TthL1–RNA	239	3.620	19	6	1.48×10^{-7}

the wild-type protein complex structure. In spite of the mutation-induced changes in the structures of the free protein, the relative arrangement of the protein and RNA and the intermolecular contact region in the complexes are well preserved in all cases. All of these TthL1–RNA complexes are stabilized by hydrogen bonds and van der Waals contacts. The total number of RNA–protein contacts and the average RNA–protein distances in the range 2.6–4.0 Å as well as the number of conserved hydrogen bonds and their average lengths are given in Table 2. These parameters are practically the same for the wild-type and mutant protein complexes. Therefore, the reduced RNA-binding ability of mutant proteins cannot be explained only by the observed changes in the structures of the complexes.

To gain further insight into the mechanism of interaction between TthL1 mutants and the 23S rRNA fragment, surface plasmon resonance (SPR) was used. At the initial stage all obtained curves were analyzed using a one-stage reaction model. This produced excellent fits ($\chi^2 < 2.5$) for the protein–rRNA complexes formed by wild-type TthL1 and the T217A and T217V mutants (Figs. 6*a*, 6*b* and 6c) but not for the complex formed by the G219V mutant ($\chi^2 = 5.6$; Fig. 6*d*). To obtain a better fit, we analyzed the last curves using a two-stage reaction model. In this model, two components form an intermediate complex with apparent association and dissociation rate constants k_{a1} and k_{d1} and a final complex with rate constants k_{a2} and k_{d2}. It appears that the formation of an intermediate complex is a quick process, which is followed by a slower transformation into the final structure, similar to the complex formed by the wild-type protein with rRNA (Supplementary Table S4). The two-stage model produces excellent fit ($\chi^2 = 1.9$) for the protein–RNA complex formed by the TthL1 G219V mutant (Fig. 6*e*).

It can be seen in Table 2 that all mutations lower the protein–RNA affinity. In the complexes formed by the T217A and T217V mutants, one intermolecular hydrogen bond formed by Thr217 that is conserved and inaccessible to solvent is lost. As a result, the dissociation rate constants increased 31–231 times compared with the wild-type protein complex. Possibly, some strained conformation in the protein–RNA interface of the T217V TthL1–rRNA complex is responsible

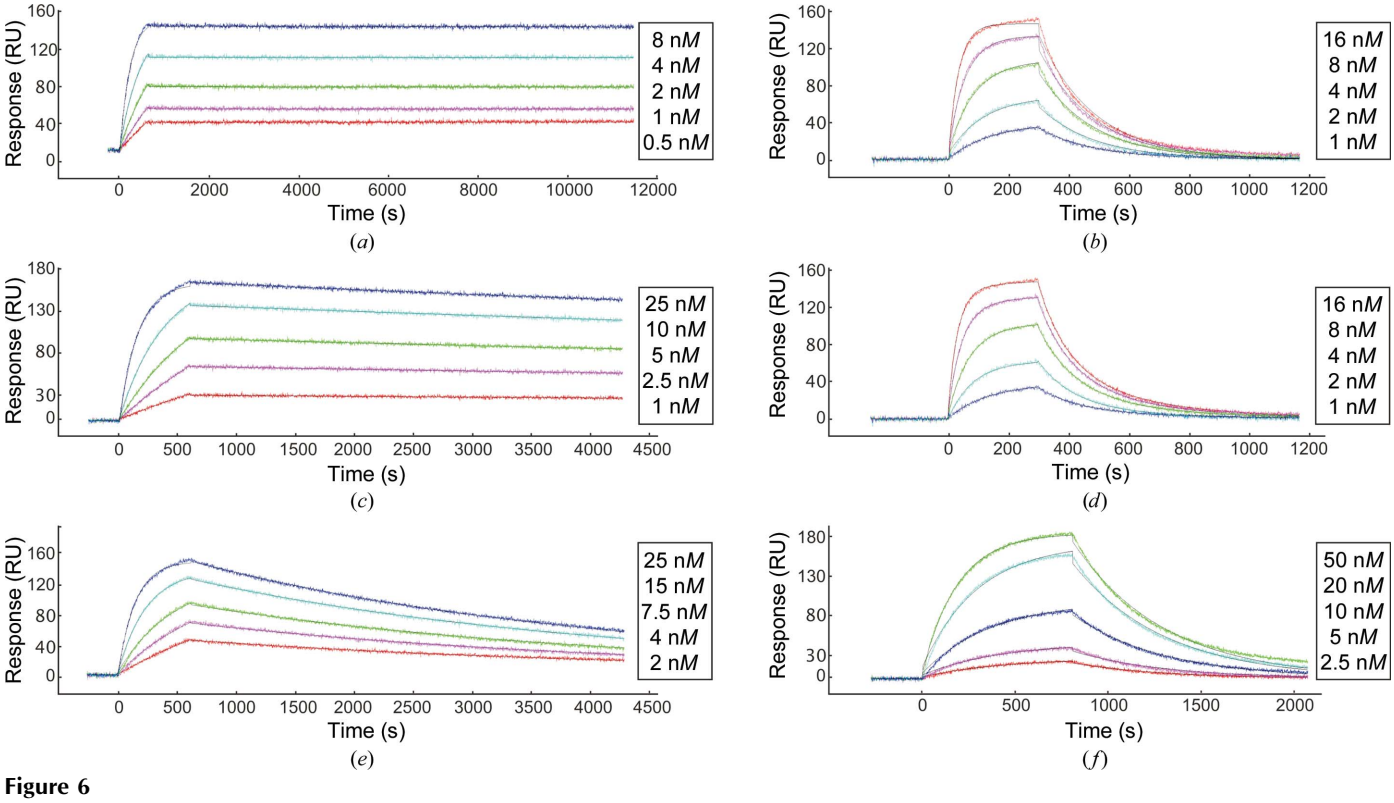

Figure 6
Sensograms showing kinetic analysis of the binding of wild-type TthL1 (*a*) and its T217A (*b*), T217V (*c*), G219V (*d*, *e*) and M218L (*f*) mutants to the 80 nt fragment of 23S rRNA. The analyte concentrations used for each data set are shown. Bold lines represent the global fit of data sets using a 1:1 model. Curves relevant to the G219V mutant were processed using one-stage (*d*) and two-stage (*e*) reaction models.

for the impairment of complex stability. The association rate constant for the wild-type protein is approximately twice that of these two mutants. In contrast to both of these complexes, in the complex formed by the G219V mutant all hydrogen bonds that are conserved and inaccessible to solvent are retained, but presumably the need for adaptation of the protein structure to RNA binding dramatically decreases the real rate of formation of the final complex.

The two-stage reaction model also produced a very good fit for the M218L TthL1–rRNA complex sensograms (Fig. 6*f*). In the free form, this mutation changes the conformation and the properties of the RNA-binding region of the protein, which should affect protein–RNA recognition. Similarly to the case of the G219V mutant, this will require an 'adjustment' of protein and rRNA complex formation through an intermediate complex that is presumably formed with a slower rate.

4. Discussion

In all TthL1–RNA complexes the protein acts as tongs, with a central part (β1) and two movable arms formed by loops β7–β8 and β9–β10 (Fig. 1*c*). Loop α2–β1 protects the β9–β10 arm from solvent, while the tongs enclose helix 77 of 23S rRNA and hold it tightly. The conserved residues of the central part (Glu42) and both arms (Asp166 and Thr217) of the tongs form hydrogen bonds to the N2 atoms of G2123, G2121 and G2124 that are inaccessible to solvent (Supplementary Table S5), corroborating their importance in determining nucleotide specificity in the interactions between TthL1 and helix 77 of 23S rRNA. The N-terminal part of helix α1 of the protein contacts helices 77 and 78, contributing to the grip of rRNA. In the RNA-free state of TthL1 (closed conformation), domain II shields the RNA-binding region and must be moved aside ('open' conformation) on complex formation. This process is accompanied by conformational changes in loop α2–β1 containing the highly conserved Phe37 (Supplementary Fig. S2). Through hydrogen bonds formed by Glu39, loop α2–β1 is connected to the β9–β10 tongs arm, which contains the highly conserved triad Thr217-Met218-Gly219.

We have studied the effect of replacing all of the residues in this triad. In the free form of the TthL1 mutants, all substitutions modified the conformation of the β9–β10 arm and its position relative to the β7–β8 region. In the RNA-bound form, the substitutions produced changes at the points of mutations, whereas the main-chain conformations were identical to those found in wild-type TthL1. In the T217A and T217V TthL1–23S rRNA complexes, either a small cavity or small bulge was formed on the protein surface. A cavity placed no obstacles to protein–RNA binding, while a bulge produces small displacements in the positions of the protein and RNA atoms. It is possible that these displacements do not require the formation of an intermediate complex (K_d is very close to that of wild-type L1; Supplementary Table S4). Therefore, the one-stage model produced a good fit for these complexes.

In contrast, the introduced defect in the G219V mutant is stabilized by hydrophobic interactions and cannot be eliminated on the transition from the closed to an open conformation of TthL1. The large bulge formed by Pro220 prevents the protein tongs from enclosing helix 77 of 23S rRNA and inhibits instant formation of the complex. In this case it is possible to suggest the following scheme for complex formation: initially the protein may contact RNA using the central part of the tongs and the β7–β8 arm, forming a complex in which the β9–β10 arm and RNA are separated by the bulge on the protein surface. The mobile N-terminus of L1 may interact with helix 78 of the rRNA fragment and attracts the protein to RNA, distorting the bulge and forcing Val219 into a position which would facilitate the formation of a structure similar to that of the wild-type complex structure. These interactions are critically important because this mutant, in contrast to wild-type TthL1 and the T217A and T217V mutants, is unable to form a specific complex either with the 55 nt rRNA containing a shortened helix 78 or with mRNA (data not shown). This suggests that if the intermediate complex is not transformed into a structure similar to that formed by wild-type L1 the final complex will probably not be formed.

On complex formation, loop α2–β1 undergoes the same conformational changes with or without domain II and shields the Thr217-Met218-Gly219 triad from solvent (Tishchenko *et al.*, 2007, 2012). In the case of the M218L mutant, the extensive hydrophobic patch formed by Phe37 and Ile218 is able to intervene in these conformational changes and to impair protein–RNA recognition. Nonetheless, compared with wild-type L1, only for this mutant is the association rate constant of protein–RNA complex formation significantly reduced (by up to two orders of magnitude; Supplementary Table S4).

All examined L1–RNA complexes show an arrangement of the relative position of domain I of TthL1 and helix 77 of 23S rRNA identical to that of the complex formed by wild-type L1. The correct arrangement of both molecules can be achieved through a one-stage or two-stage binding event. In all examined cases, the formation of the intermediate complexes can be associated with additional interactions between loops α2–β1 and β9–β10, which have to be eliminated prior to formation of the final complex. TthL1 shows high affinity for 23S rRNA, and even its mutants with substitutions in the highly conserved triad Thr217-Met218-Gly219 are able to bind rRNA. As the L1–RNA interfaces are very similar in bacteria and archaea (Tishchenko *et al.*, 2012; Nikulin *et al.*, 2003), it seems that the rigid body formed by protein L1 and helix 77 of 23S rRNA should be conserved in the L1 stalks of the bacterial and archaeal ribosomes and is essential for ribosome function.

The analysis of the protein–RNA interfaces of the complexes formed by wild-type TthL1 and its mutants presented here shows that the total number of protein–RNA contacts and hydrogen bonds is very similar (Table 2, Supplementary Table S5). At the same time, the wild-type complex has the highest protein–RNA affinity; this is impaired in the mutant complexes. This reduction can be associated with both protein–RNA recognition and complex stability and may be lower by as much as five orders of magnitude (in the M218L TthL1–rRNA complex). This suggests that the total number of protein–RNA contacts and hydrogen bonds cannot

be used as a measure of the protein–RNA affinity, at least in the case of complexes formed by TthL1 mutants.

This work was supported by the Russian Foundation for Basic Research (No. 14-04-00414) and the Program of RAS on Molecular and Cellular Biology. We are indebted to Dr Alexei Kazakov (Institute for Biological Instrumentation of the Russian Academy of Sciences, Pushchino, Russia) for assistance with SPR measurements.

References

Afonine, P. V., Grosse-Kunstleve, R. W., Echols, N., Headd, J. J., Moriarty, N. W., Mustyakimov, M., Terwilliger, T. C., Urzhumtsev, A., Zwart, P. H. & Adams, P. D. (2012). *Acta Cryst.* D**68**, 352–367.

Emsley, P., Lohkamp, B., Scott, W. G. & Cowtan, K. (2010). *Acta Cryst.* D**66**, 486–501.

Fei, J., Bronson, J. E., Hofman, J. M., Srinivas, R. L., Wiggins, C. H. & Gonzalez, R. L. Jr (2009). *Proc. Natl Acad. Sci. USA*, **106**, 15702–15707.

Hooft, R. W. W., Vriend, G., Sander, C. & Abola, E. E. (1996). *Nature (London)*, **381**, 272.

Kabsch, W. (2010). *Acta Cryst.* D**66**, 125–132.

Katsamba, P. S., Park, S. & Laird-Offringa, I. A. (2002). *Methods*, **26**, 95–104.

Kostareva, O., Tishchenko, S., Nikonova, E., Kljashtorny, V., Nevskaya, N., Nikulin, A., Sycheva, A., Moshkovskii, S., Piendl, W., Garber, M. & Nikonov, S. (2011). *J. Mol. Recognit.* **24**, 524–532.

Laskowski, R. A., MacArthur, M. W., Moss, D. S. & Thornton, J. M. (1993). *J. Appl. Cryst.* **26**, 283–291.

Liu, H. & Naismith, J. H. (2008). *BMC Biotechnol.* **8**, 91–100.

McCoy, A. J., Grosse-Kunstleve, R. W., Storoni, L. C. & Read, R. J. (2005). *Acta Cryst.* D**61**, 458–464.

Murshudov, G. N., Skubák, P., Lebedev, A. A., Pannu, N. S., Steiner, R. A., Nicholls, R. A., Winn, M. D., Long, F. & Vagin, A. A. (2011). *Acta Cryst.* D**67**, 355–367.

Nevskaya, N., Tishchenko, S., Fedorov, R., Al-Karadaghi, S., Liljas, A., Kraft, A., Piendl, W., Garber, M. & Nikonov, S. (2000). *Structure*, **8**, 363–371.

Nevskaya, N., Tishchenko, S., Gabdoulkhakov, A., Nikonova, E., Nikonov, O., Nikulin, A., Platonova, O., Garber, M., Nikonov, S. & Piendl, W. (2005). *Nucleic Acids Res.* **33**, 478–485.

Nevskaya, N., Tishchenko, S., Volchkov, S., Kljashtorny, V., Nikonova, E., Nikonov, O., Nikulin, A., Köhrer, C., Piendl, W., Zimmermann, R., Stockley, P., Garber, M. & Nikonov, S. (2006). *J. Mol. Biol.* **355**, 747–759.

Nikonova, E. Y., Volchkov, S. A., Kljashtorny, V. G., Tishchenko, S. V., Kostareva, O. S., Nevskaya, N. A., Nikonov, O. S., Gabdoulkhakov, A. G., Nikulin, A. D., Davydova, N. L., Streltsov, V. A., Garber, M. B. & Nikonov, S. V. (2007). *Mol. Biol. (Mosk.)*, **41**, 688–696.

Nikonov, S., Nevskaya, N., Eliseikina, I., Fomenkova, N., Nikulin, A., Ossina, N., Garber, M., Jonsson, B. H., Briand, C., Al-Karadaghi, S., Svensson, A., Aevarsson, A. & Liljas, A. (1996). *EMBO J.* **15**, 1350–1359.

Nikulin, A., Eliseikina, I., Tishchenko, S., Nevskaya, N., Davydova, N., Platonova, O., Piendl, W., Selmer, M., Liljas, A., Drygin, D., Zimmermann, R., Garber, M. & Nikonov, S. (2003). *Nature Struct. Biol.* **10**, 104–108.

Tishchenko, S., Gabdulkhakov, A., Nevskaya, N., Sarskikh, A., Kostareva, O., Nikonova, E., Sycheva, A., Moshkovskii, S., Garber, M. & Nikonov, S. (2012). *Acta Cryst.* D**68**, 1051–1057.

Tishchenko, S., Kljashtorny, V., Kostareva, O., Nevskaya, N., Nikulin, A., Gulak, P., Piendl, W., Garber, M. & Nikonov, S. (2008). *J. Mol. Biol.* **383**, 301–305.

Tishchenko, S., Nikonova, E., Kljashtorny, V., Kostareva, O., Nevskaya, N., Piendl, W., Davydova, N., Streltsov, V., Garber, M. & Nikonov, S. (2007). *Nucleic Acids Res.* **35**, 7389–7395.

Tishchenko, S., Nikonova, E., Kostareva, O., Gabdulkhakov, A., Piendl, W., Nevskaya, N., Garber, M. & Nikonov, S. (2011). *Acta Cryst.* D**67**, 1023–1027.

Tishchenko, S., Nikonova, E., Nikulin, A., Nevskaya, N., Volchkov, S., Piendl, W., Garber, M. & Nikonov, S. (2006). *Acta Cryst.* D**62**, 1545–1554.

Trabuco, L. G., Schreiner, E., Eargle, J., Cornish, P., Ha, T., Luthey-Schulten, Z. & Schulten, K. (2010). *J. Mol. Biol.* **402**, 741–760.

Unge, J., Al-Karadaghi, S., Liljas, A., Jonsson, B. H., Eliseikina, I., Ossina, N., Nevskaya, N., Fomenkova, N., Garber, M. & Nikonov, S. (1997). *FEBS Lett.* **411**, 53–59.